Progress in Structural Engineering, Mechanics and Computation, Zingoni (ed.)
© 2004 Taylor & Francis Group, London, ISBN 90 5809 568 1

Effect of some parameters on the optimum height of planar CHS trusses with parallel chords

K. Jármai
Faculty of Mechanical Engineering, University of Miskolc, Miskolc, Hungary

J.A. Snyman
Department of Mechanical Engineering, University of Pretoria, Pretoria, South Africa

J. Farkas
Faculty of Mechanical Engineering, University of Miskolc, Miskolc, Hungary

ABSTRACT: The optimum design of planar trusses is shown in this study by means of two novel and interrelated constrained gradient-based optimization techniques, namely the Leap-frog method and the Dynamic-Q method. In the optimization the height and the cross-sectional dimensions are optimized using circular hollow sections (CHS) for minimum volume. The effect of several truss parameters, such as loads, number of fields, has been investigated during the optimization. Using the optimized height, significant mass and cost savings can be achieved in the design stage. This is in contrast to the current routine and design practice in which the truss height is taken proportional to the span length, and which does not give an optimal solution with minimum mass.

KEYWORDS: Structural optimization, tubular trusses, gradient-based optimization, approximation methods.

1 INTRODUCTION

Tubular trusses are getting more popular in design practice. Using hollow sections a relatively large strength/mass ratio can be achieved. The aim of this study is to present a design methodology, through which the optimum truss height and cross-sectional dimensions may be determined for several truss parameters such as loads, number of fields, etc. A previous study has indicated that, using optimized heights, significant mass and cost savings can be achieved in the design stage (Farkas & Jármai 2003). The present study emphasizes that the current practice of selecting the truss height (h) proportional to the span length (L) by setting, for example, $h = L/10$ to $L/20$, does not give the optimal solution. Designers should rather *simultaneously* optimize the height and cross-sectional dimensions for actual loads, span length and type of bracing.

The two *constrained* optimization algorithms have been used: the LFOPC Leap-frog method (Snyman 2000) and the Dynamic-Q (Snyman & Hay 2002) method. These methods are gradient-based and have the common and unique property, that no explicit line searches are required. The first method searches directly for a local minimum via a computed descent trajectory. In the second approach a sequence of *approximate* optimization subproblems are considered, which are successively solved via the first trajectory method.

Both methods solve constrained problems of the general form:

$$\underset{w.r.t.\ \mathbf{x}}{\text{minimize}} \quad f(\mathbf{x}),\ \mathbf{x} = [x_1, x_2, \ldots x_n]^T \in R^n \tag{1}$$

subject to the inequality and equality constraints:

$$\begin{aligned} g_j(\mathbf{x}) &\le 0, \quad j = 1,2,\ldots,m \\ h_j(\mathbf{x}) &= 0, \quad j = 1,2,\ldots,r \end{aligned} \tag{2}$$

where the objective function $f(\mathbf{x})$, and the constraint functions $g_j(\mathbf{x})$ and $h_j(\mathbf{x})$, are scalar functions of the

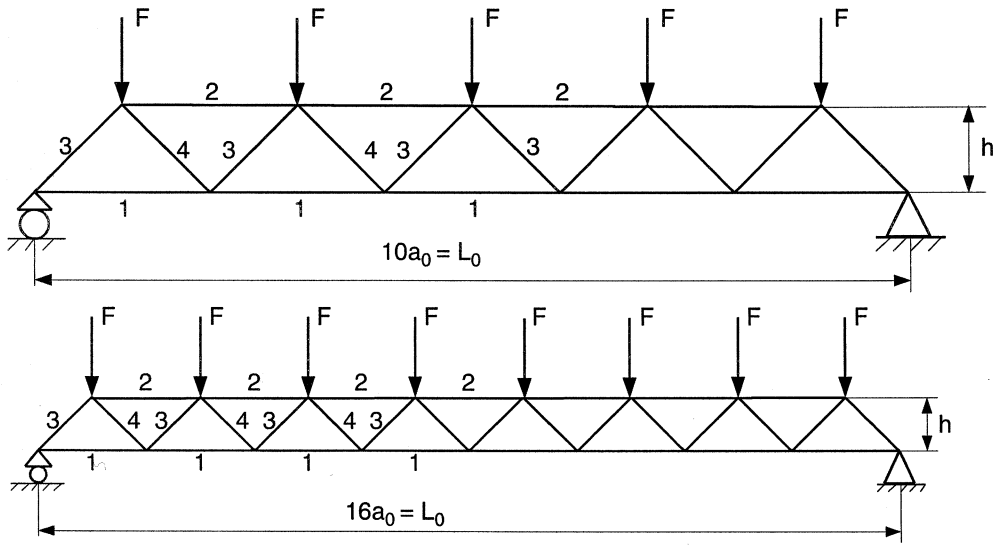

Figure 1. Planar five-field ($n_f = 5$) and eight-field ($n_f = 8$) trusses with parallel chords. The numbering relates to groups of members of identical cross-section.

real column vector **x**. Constraints are handled via the unconstrained minimization of the penalty function

$$P(\mathbf{x}) = f(\mathbf{x}) + \sum_{j=1}^{r} \rho_j h_j^2(\mathbf{x}) + \sum_{j=1}^{m} \beta_j g_j^2(\mathbf{x}) \qquad (3)$$

2 MINIMUM VOLUME DESIGN OF A TUBULAR TRUSS OF PARALLEL CHORDS

2.1 *Optimal design problem*

The specific engineering problem to be considered here is the determination of the minimum weight design of a planar and statically determinate K-type truss with parallel chords and gap joints, welded from circular hollow section (CHS) rods (see Figs 1 and 2). The optimization is to be carried out with respect to design variables that include, for each structural group (see Section 2.2), the cross-sectional diameter and wall thickness and the height between the chords. Previously the truss height was a design parameter and the design variables in the optimization were the diameters and thicknesses (Jármai 1998). The simultaneous and continuous optimization, with respect to tube dimensions and inter-chord height, is carried out here for different choices of half-chord lengths and different loads, for both the 5 field and 8 field cases.

The structural members (tubular rods) are divided into four groups, the members of each group having identical lengths and cross-sections. The different groups respectively consist of (1) lower chord members, (2) upper chord members, (3) compression braces, and (4) tension braces as indicated in Figure 1. Each group i, $i = 1, 2, 3, 4$, has two design variables,

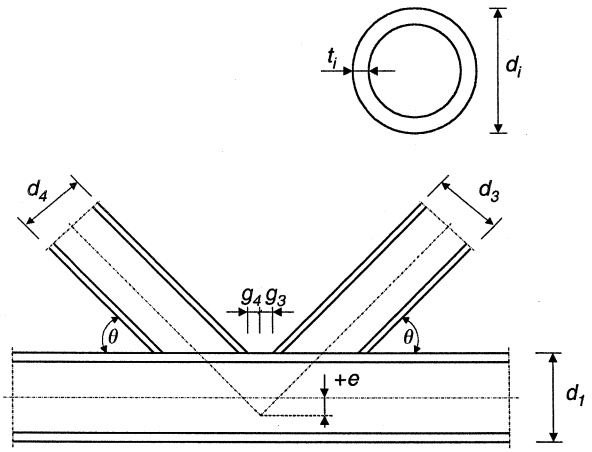

Figure 2. K-type gap joint with eccentricity e.

namely the diameter d_i and wall thickness t_i of the corresponding tube. The fixed parameters for a particular structure are the half-chord member length a_o (see Figure 1), the number of fields n_f, corresponding to the number of lower chord members, and the vertical load F at each of the upper nodes. The total span is therefore $L_o = 2a_o n_f$ and the total load $F_T = (n_f - 1)F$.

2.2 *Design variables*

For a given set of fixed parameters, a_o, n_f and F, the vector **x** of *design variables* is given by

$$\mathbf{x} = [x_1, x_2, \ldots, x_9]^T = [d_1, t_1, d_2, t_2, d_3, t_3, d_4, t_4, \omega]^T \qquad (4)$$

where $x_9 = \omega = \frac{h}{a_o}$.

2.3 *Objective function*

For given cross-sections and value of $\omega = h/a_o$ the objective function considered here is the structural volume V scaled by division by $2\pi a_o$ and can be expressed as follows:

$$f(x) = \frac{V}{2\pi a_o} = c_1(d_1 - t_1)t_1 + c_2(d_2 - t_2)t_2 + \\ + c_3\sqrt{\omega^2+1}(d_3 - t_3)t_3 + c_4\sqrt{\omega^2+1}(d_4 - t_4)t_4, \quad (5)$$

where the values of the coefficients $c_i, i = 1, \ldots, 4$ depend on the number of fields n_f being considered: $c_1 = n_f$, $c_2 = n_f - 1$, and for n_f odd $c_3 = (n_f + 1)/2$, $c_4 = (n_f - 1)/2$, and for n_f even $c_3 = c_4 = n_f/2$.

2.4 *Constraints*

It is required to minimize the volume given by expression (5), subject to stability and fabrication constraints as set out in the following sub-sections. All members are made from steel Fe 510 with ultimate strength $f_u = 510$ MPa and yield stress $f_y = 355$ MPa. The load F in kN are applied as shown in Figure 1 where the factored value of the static forces are used.

Only inequality constraints arise in this study. They are listed in the standard form (2), $g_j(\mathbf{x}) \le 0$ below (member forces are given only for 5 fields).

Local buckling constraints (1st–4th) for all sections according to Wardenier et al. (1991) are

$$g_j(\mathbf{x}) = d_j/t_j - 50 \le 0, \qquad (j = 1,\ldots 4). \quad (6)$$

Overall buckling constraints (5th–6th) for compression members according to EC3 are as follows (Rondal et al. 1992):

$$\frac{S_{j\max}}{\pi(d_j - t_j)t_j} \le \frac{\chi_j f_y}{\gamma_{M1}}; \quad (j = 2, 3) \quad (7)$$

where

$$\chi_j = \frac{1}{\phi_j + \sqrt{\phi_j^2 - \bar{\lambda}_j^2}}; \quad \phi_j = 0.5\left[1 + 0.34(\bar{\lambda}_j - 0.2) + \bar{\lambda}_j^2\right] \quad (8)$$
$$(j = 2, 3)$$

$$\bar{\lambda}_j = \frac{\lambda_j}{\lambda_E} = \frac{K_j L_j}{\lambda_E r_j}. \qquad (j = 2, 3) \quad (9)$$

The member forces for the upper chord: $j = 2$ and for the compression braces: $j = 3$ respectively

$$S_{2\max} = \frac{6F}{\omega}; \quad S_{3\max} = \frac{2.5F}{\omega}\sqrt{\omega^2+1}; \quad (10)$$

With $E = 2.1 \times 10^5$ MPa and $f_y = 355$ MPa

$$\lambda_E = \pi\sqrt{E/f_y} = 76.4091, \quad \gamma_{M1} = 1.1;.$$

$K_2 = 0.9$ and $K_3 = 0.75$ are the end restraint factors according to Rondal et al. (1992), $r_j = (d_j - t_j)/\sqrt{8}$, $(j = 2, 3)$ are the radii of gyration.

Stress constraint (7th–8th) for tension members are

$$\frac{S_{j\max}}{\pi(d_j - t_j)t_j} - \frac{f_y}{\gamma_{Mo}} \le 0; \ (j = 1, 4) \quad (11)$$

The member forces for the lower chord: $(j = 1)$ and for the tension brace: $(j = 4)$ respectively

$$S_{1\max} = \frac{6.5F}{\omega}; \quad S_{4\max} = \frac{1.5F}{\omega}\sqrt{\omega^2+1}. \quad (12)$$

where $\gamma_{Mo} = 1.1$;

*Size constraints (9th–*12th): in order to ease the fabrication the diameter of braces should be smaller than those of chords:

$$d_j - 0{,}92d_k \le 0; \ (j = 3, 4, k = 1, 2) \quad (13)$$

$$g_3 = 0.05\, d_1 \ \text{ and } \ g_4 = 0.05\, d_2 \quad (14)$$

Prescription for the joint eccentricity (13th–14th constraints): to avoid too large additional bending moment in the vicinity of nodes is as follows (Fig. 2):

$$e - 0.25d_j \le 0; \qquad (j = 1, 2) \quad (15)$$

The geometry constraints (15th–16th) are given by:

$$\frac{d_3}{2}\sqrt{\omega^2+1} + d_j(0.05\omega - 0.75) \le 0, \quad (j = 1, 2) \quad (16)$$

Constraints on chord plastification (17th–18th) in the joint of rods 1 and 3 and of rods 2 and 3:

$$S_{3\max} - S_{3j}^* \le 0, (j = 1 \text{ for rod 1 and } j = 2 \text{ for rod 2}) \quad (17)$$

where

$$S_{3j}^* = \frac{f_y t_j^2}{\sin\theta}\left(1.8 + 10.2\frac{d_3}{d_j}\right) f_j(\gamma_j, g_j'), \quad (18)$$

$$f_j(\gamma_j, g_j') = \gamma_j^{0.2}\left[1 + \frac{0.024\gamma_j^{1.2}}{\exp(0.5g_j' - 1.33) + 1}\right]; \ \gamma_j = \frac{d_j}{2t_j} \quad (19)$$

$$g_j' = g_j/t_j; \ \text{we assume that } \ g_j = g_3 + g_4 = 0.1d_j \quad (20)$$

Constraints on chord plastification for joints of rods 1–4 and 2–4 can be formulated similarly to Equations

18–20, therefore these constraints are not detailed here (*19th–20th constraints*).

Constraints on static strength of welded joints (*21st–22nd*) between chords and braces according to EC3 is

$$\sqrt{\sigma_{\perp}^2 + 3\left(\tau_{\perp}^2 + \tau_{II}^2\right)} \le f_u / \left(\beta_w \gamma_{MW}\right), \tag{21}$$

$$f_u = 510\,\text{MPa}, \quad \beta_w = 0.9, \quad \gamma_{Mw} = 1.25. \tag{22}$$

From the force S in a brace the following stress components arise in welds:

$$\sigma_{\perp} = \tau_{\perp} = \frac{S\sin\theta}{\pi d a_w} \cdot \frac{\sqrt{2}}{2}; \quad \tau_{II} = \frac{S\cos\theta}{\pi d a_w}, \tag{23}$$

where a_w is the fillet weld dimension. Substituting Equation 23 into Equation 21 we get

$$\frac{S}{\pi d a_w}\sqrt{\frac{2\omega^2+3}{\omega^2+1}} - 453 \le 0. \tag{24}$$

For the maximal value of a_w the corresponding brace thickness can be taken. This constraint should be fulfilled for S_3 and S_4 (*22nd–23rd constraints*).

3 NUMERICAL RESULTS

The continuous optimization were done for two cases, namely for the number of fields $n_f = 5$ and for $n_f = 8$, and in each case for different half-chord member lengths a_0. For each choice of a_0 the optimization was performed for a range of different nodal static forces F. These results are integrated in the following subsections. The results of the discretization of the continuous solution for two particular examples are presented in sub-section 3.3.

3.1 *Continuous results for five-field*

For 5 fields the optimization was carried out for $a_0 = 2000$, 3000 and 4000 mm, and in each case for different nodal static forces ranging from $F = 200$ kN, in steps of 200 kN to a maximum of $F = 1600$ kN. For each choice of the fixed parameters a_0 and F, the optimum solution $\mathbf{x}^*$, which includes ω^*, and the corresponding minimum weight $f(\mathbf{x}^*) = V^*/(2\pi a_o)$, was determined by both the LFOPC and Dynamic-Q algorithms. For all practical purpose the two algorithms give identical optima on convergence (typically the relative differences between the respective optimum values of $f(\mathbf{x}^*)$ is less than 10^{-7}). Figure 3(a) depicts, for each choice of a_0, the variation of $f^* = f(\mathbf{x}^*)$ with F, and Figure 3(b) gives the corresponding variation of ω^* with F.

The detailed results for a typical five-field optimization run, namely for $a_0 = 3000$ mm and $F = 1000$ kN are given in Table 1. The optimal dimensions listed are the same for both algorithms.

Table 1. Optimization results (in mm) for typical five-field case: $a_0 = 3000$ mm and $F = 1000$ kN.

$d_1^* = 256.6$; $t_1^* = 20.44$; $d_2^* = 286.1$; $t_2^* = 20.41$;
$d_3^* = 211.0$; $t_3^* = 19.22$; $d_4^* = 150.7$; $t_4^* = 13.50$;
and $\omega^* = \frac{h}{a_o} = 1.328$.
Active constraints $g_j(\mathbf{x}^*) \cong 0$: $j = 5, 6, 7, 8, 13, 15, 17, 18$, with $\max\lvert g_j(\mathbf{x}^*)\rvert = 7 \times 10^{-9}$, and *no* active side constraints.

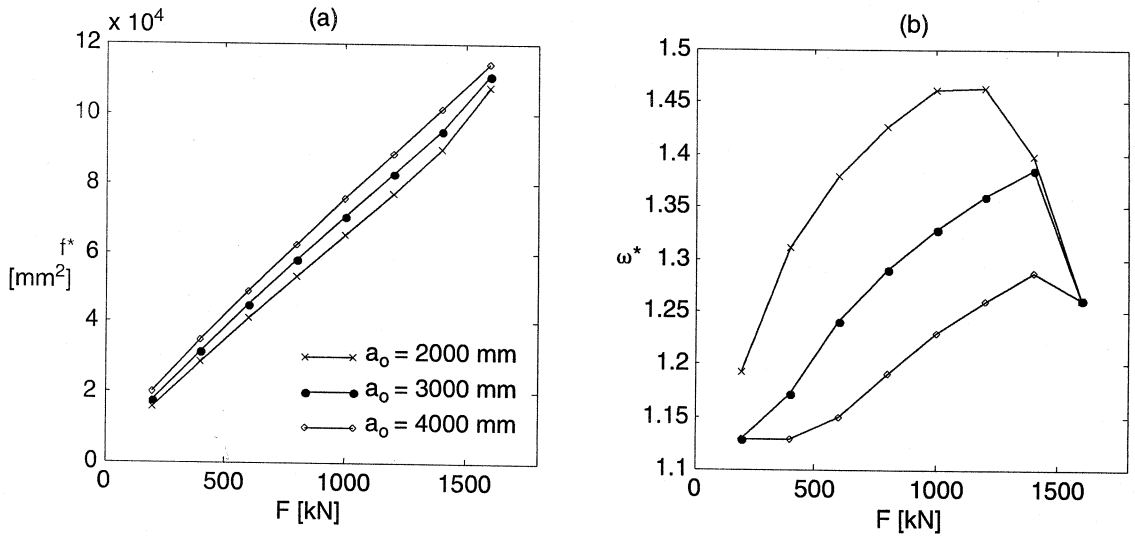

Figure 3. For $n_f = 5$ fields and for different choices of a_0: (a) the variation of $f^* = V^*/(2\pi a_o)$ with F, and (b) the variation of ω^* with F.

3.2 *Continuous results for eight-field*

For 8 fields the optimization was also carried out for $a_0 = 2000$, 3000 and 4000 mm, and in each case for different nodal static forces static forces $F = 50$ kN, 100 kN, 200 kN and in further steps of 200 kN to a maximum of $F = 1000$ kN. For each choice of the fixed parameters a_0 and F, the optimum solution $\mathbf{x}^*$, which includes ω^*, and the corresponding minimum weight $f(\mathbf{x}^*)$, was determined by both the LFOPC and Dynamic-Q algorithms. Again for all practical purpose the two algorithms gave identical optima on convergence (the relative differences between the respective optimum values of $f(\mathbf{x}^*)$ being less than 10^{-7}. Figure 4 gives the corresponding variation of ω^* with F.

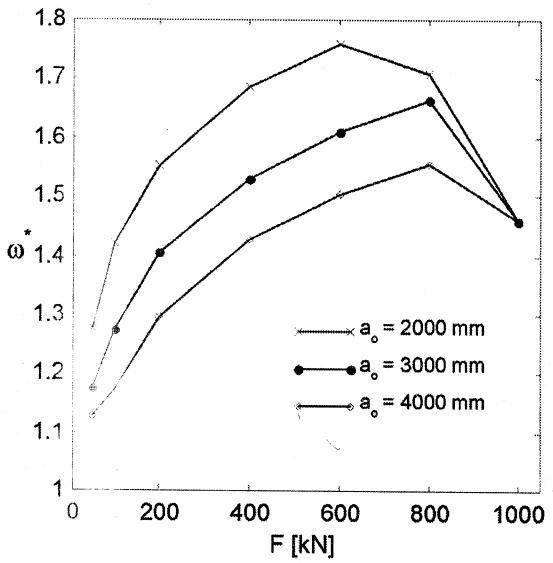

Figure 4. For $n_f = 8$ fields the variation of ω^* with F for different choices of a_0.

Table 2. Optimization results (in mm) for typical eight-field case: $a_0 = 2000$ mm and F = 800 kN.

$d_1^* = 321.0$ $t_1* = 25.00$ $d_2^* = 339.4$ $t_2^* = 24.85$;
$d_3^* = 215.7$ $t_3^* = 20.77$ $d_4^* = 211.6/197.3$;
$t_4^* = 13.88/15.06^{\#}$ *and* $\omega^* = \frac{h}{a_o} = 1.706$
Active constraints $g_j(\mathbf{x}^*) \cong 0$: $j = 5, 6, 7, 8, 13, 15, 17, 18$, with $\max|g_j(\mathbf{x}^*)| = 6 \times 10^{-9}$, and *active* upper bound:
$t_1^* = \hat{t}_1 = 25$

3.3 *Results for the discretization of continuous optimum solutions*

Discretization of the physical dimensions is carried out for two examples, respectively corresponding to the five-field case in Table 1 and the eight-field case in Table 2. The results are shown in Table 3. In both cases the value of ω, which need not correspond to a discrete value, was kept at its continuously determined optimum value.

The discretization of the dimensions increases the discrete optimum objective function value relative to the continuous optimum by 4% and 2% for the five and eight field cases respectively. These increases are acceptably small.

4 DISCUSSION OF RESULTS AND CONCLUSION

The aim of this study, namely the establishment of a methodology for determining the dependence of the optimum truss height and optimum cross-sectional dimensions on loads and span length has been achieved. For example, results obtained by the method for the five field and eight field cases, and as depicted in Figures 3 and 4, illustrate the fact that the optimal $\omega = h/a_0$ ratio varies in a non-linear manner between 1.12 and 1.75, depending on the load. It is also clear, that an increase in a_0 results in an increase in the optimum volume and mass of the truss. Also, the volume appears to be linearly proportional to the loading. If the loading is the same, the optimal ω is larger for the smaller nodal distance ($a_0 = 2000$), with the corresponding h even smaller than that for the greater nodal distance ($a_0 = 4000$). Thus it can be concluded that the routine design practice of simply taking the truss height proportional to span length, is not to be recommended, since it does not give a minimum mass design within the specified constraints.

The two optimization algorithms used in this study, gave almost identical results for the 48 continuous optimization runs performed in producing the results shown in Figures 3 and 4. This gives confidence in the results obtained.

Table 3. Discrete optimum dimensions (in mm) for the five- and eight field structures.

Field number	$d_1 \times t_1$	$d_2 \times t_2$	$d_3 \times t_3$	$d_4 \times t_4$	ω	$f(\mathbf{x}^*)(\text{mm}^2)$
5	260 × 21	290 × 21	210 × 20	150 × 14	1.328	72972.2
8	330 × 25	340 × 25	220 × 21	210 × 14	1.706	170891

ACKNOWLEDGEMENT

The research work was supported by the Hungarian Scientific Research Foundation grants OTKA T38058 and T37941. The project was also supported by, the Hungarian-South African Intergovernmental S&T co-operation program. The Hungarian partner is the Ministry of Education, R&D Deputy Undersecretary of State, and the South African partner is the National Research Foundation.

REFERENCES

Farkas J. & Jármai, K. 2003. *Economic Design of Metal Structures*, Millpress, Rotterdam, 340 p. ISBN 90 77017 99 2

Jármai, K. 1998. *Topology optimization of tubular structures*, Chapter 5 in *Mechanics and Design of Tubular Structures*, Springer Verlag, Edited by K. Jármai & J. Farkas, pp. 225–284. ISBN 3-211-83145-2

Rondal, J., Würker, K-G. et al. 1992. *Structural stability of hollow sections*. Köln, TÜV Rheinland.

Snyman J.A. 2000. The LFOPC leap-frog method for constrained optimization. *Computers Math. Applic.*, Vol. 40, 1085–1096.

Snyman J.A. & Hay A.M. 2002. The Dynamic-Q optimization method: an alternative to SQP? *Computers Math. Applic.*, Vol. 44, 1589–1598.

Wardenier, J., Kurobane, Y. et al. 1991. *Design guide for circular hollow section joints under predominantly static loading*. Köln, TÜV Rheinland.